

HYDROGRAPHIC LIDAR IN SPACE: FERMAT'S PRINCIPLE AS AN ANALYTICAL APPROACH FOR ATMOSPHERIC RADIATIVE TRANSFER SIMULATION

Rainer Reuter and Oliver Zielinski

Carl von Ossietzky Universität Oldenburg
Fachbereich Physik, D-26111 Oldenburg, Germany
r.reuter@las.physik.uni-oldenburg.de
o.zielinski@las.physik.uni-oldenburg.de

ABSTRACT

Recently, measuring water-column parameters with fluorescence lidar at flight altitudes higher than 300 m has met with increasing interest. The feasibility of such measurements using platforms at altitudes of up to 800 km are studied. This would allow to operate the instrument as an attachment to atmospheric lidars.

A simulation is presented, using Fermat's principle as an analytical approach to describe the radiative transfer processes in the atmosphere. A cloudless and stratified atmosphere with various aerosol and ozone conditions is taken into consideration. Particular emphasis is put onto the radiative transfer at wavelengths which are relevant to hydrographic fluorescence measurements. A number of results are presented concerning the geometrical aspects of radiative transfer through the atmosphere, such as optimised lidar parameters and the effect of dispersion.

Finally some features of a proposed hydrographic lidar in space are presented. It is outlined that data simultaneously measured with an atmospheric lidar allow to correct the fluorescence signal for atmospheric effects, yielding quantitative results of fluorescent matter concentrations in the sea.

Keywords: hydrographic lidar, laser fluorosensor, ocean monitoring, radiative transfer, gelbstoff, Fermat

1 INTRODUCTION

Ocean monitoring of biological and chemical components like planktonic chlorophyll in algae or gelbstoff (or yellow substance, chromophoric dissolved organic matter) is relevant on basin-wide or even global scales. Especially in the context of global carbon flux estimations and climatological modelling efforts, the ocean as a carbon sink and the related phytoplankton distribution have come into focus. Passive remote sensing instruments like SeaWiFS or OCTS estimate biomass from ocean color data [7,17]. Other sensors provide additional hydrographic information like sea surface temperature (SST) and sea surface elevation from which information on currents and upwelling processes can be deduced.

However, certain oceanic parameters are difficult to detect with passive remote sensing instruments. Gelbstoff is one example since it is present in open ocean (case 1) waters at too low concentrations to affect ocean colour. Its measurement over large scales would be of high interest since it plays an important role in the global carbon cycle [4]. As a second example, CZCS images from higher latitudes (e.g. the North Sea) show high phytoplankton pigment estimations during the whole time of operation (Nov.'78 - June'86) even at wintertime, which is an artefact due to high seston and gelbstoff concentrations [1].

Using the specific molecular fluorescence of these substances allows their measurement with active laser fluorosensors. Theory and application of these instruments have been extensively described in the literature [5,6,14,16]. A brief description of signals from natural organic compounds of seawater, like gelbstoff and phytoplankton chlorophyll *a* will be given

in the following section. Ocean monitoring with airborne instruments is routinely carried out in coastal zones. However, this would be difficult to establish on global scales, especially over extended time periods. Therefore, the feasibility of active fluorescence lidar measurements from altitudes of up to 800 km has met with increasing interest, since they would allow large-scale and continuous surveys.

2 FLUORESCENCE MEASUREMENTS OF BIOOPTICAL PARAMETERS

The optical characteristics of organic substances include wavelength specific absorption as well as fluorescence. Detectable components cover gelbstoff, chlorophyll *a*, and other phytoplankton pigments like phycoerythrin, fucoxanthin and fucoyanin [3,15]. In this paper only gelbstoff and chlorophyll *a* are considered. Fig. 1 shows a typical emission spectrum of coastal (case 2) seawater containing gelbstoff and algae, taken with a laboratory instrument ($\lambda_{ex} = 308$ nm). One finds:

- The water Raman peak at 344 nm resulting from inelastic scattering at H₂O molecules (with a Stokes shift of ~ 3400 1/cm).
- A spectrally broad fluorescence of gelbstoff with a characteristic maximum at 420 nm. Absorption of gelbstoff decreases with increasing wavelength and thus leads to high fluorescence intensities with UV excitation.
- Chlorophyll *a* fluorescence from photosystem II at about 685 nm.

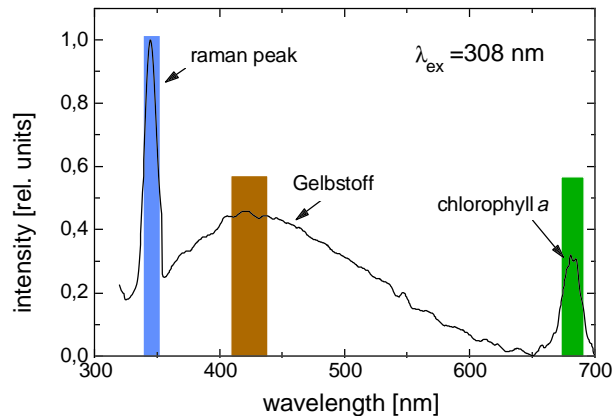


Fig. 1. Fluorescence spectrum of a seawater sample (case 2 water) containing phytoplankton and gelbstoff. Excitation wavelength: 308 nm.

Table 1 compares a number of parameters at four selected excitation wavelengths. The Raman scatter efficiency has been calculated from the Raman

scattering coefficient of water, having a λ^{-4} wavelength dependence like Rayleigh scattering [8]. Gelbstoff and chlorophyll *a* fluorescence efficiencies have been derived from laboratory experiments. They depend on the type of water and class of algae. Case 2 water samples from the German Bight were used, containing terrestrial compounds of gelbstoff. The highest fluorescence efficiency of chlorophyll *a* is at 420 nm excitation. Its absorption gap from 470 nm to 660 nm results in the low efficiency of the 532 nm excitation. However, depending on the class of algae there are different absorption characteristics due to a variety of pigments involved (e.g. carotene). Thus further investigations are planned for classification of spectral signatures from these substances.

Table 1: Efficiency of signals as a function of the excitation wavelength, in relative units.

Ex. wavelength [nm]	270	308	355	532
Raman peak [nm]	297	344	404	650
Raman efficiency	1.00	0.59	0.33	0.07
Gelbstoff flu. eff.	1.00	0.53	0.31	--
Chlorophyll <i>a</i> flu. eff.	0.40	0.72	0.76	0.06

3 MEASUREMENTS FROM SPACE

While airborne fluorosensing of maritime pollution is carried out routinely in coastal zones, this method is not yet available for measurements in larger oceanic regions. However, global monitoring programmes like e.g. the Earth Observing System EOS call for a long-term and large-scale investigation of oceanographic processes in the world oceans. Some of the parameters to be measured in these programmes can be assessed with hydrographic lidar in space. The objective of this section is to present a simulation of such an instrument, to show up solutions of specific problems and to outline the potential of a combined hydrographic/atmospheric lidar in space.

3.1 Radiative transfer in the atmosphere

Possible spaceborne platforms for a hydrographic lidar include the Space Shuttle at 300 km, space stations like MIR at 400 km and satellites on lower earth orbits of up to 800 km. From these altitudes the laser beam and the detected fluorescence of a lidar are subject to atmospheric influences that weaken and deflect the signal. In addition there exists a solar

induced background signal, strongly depending on actual weather conditions, and on the angle between sun and detector. The signal-to-background ratio is essential for information retrieval and it will be important to improve this ratio by technical progress (see Bartsch et al. [2] for a detailed study of the laser-induced-signal to solar-induced-background ratio). Possible sources of atmospheric influences for the optical information in the visible and near ultra-violet region are:

- Rayleigh scattering, with its λ^{-4} dependence.
- Absorption by ozone (O_3) - especially below 320 nm this factor is considerably high, which makes an excitation wavelength unsuitable for atmospheric transmission through the ozone layer.
- Attenuation by tropospheric and stratospheric aerosols.

In addition to these well-known effects [10, 11], there are two factors that will be examined in this simulation. A hydrographic lidar in space will change its position during the time of light propagation in the atmosphere, thus a compensation of movement effects will be necessary¹. On the other hand, a beam of light started under a laser-zenith-angle $\neq 0^\circ$ is manipulated by the variable refraction index of air. This results in a so-called *slant path* and by modelling the radiative transfer in the atmosphere it is possible to calculate the exact deviation and attenuation of an optical signal for a given atmospheric situation.

3.2 Simulation of a hydrographic lidar-in-space

In this simulation a cloudless and horizontally stratified atmosphere is considered. The US Standard Atmosphere of 1962 [11] with additional information on ozone and aerosols is applied. The refractive index $n(z)$ at an altitude z is calculated as a function of the temperature $T(z)$, the partial pressure of air $p(z)$, the partial pressure of water vapor $p_{H_2O}(z)$, and the wavelength λ using the equation by McClatchey and Selby [12]:

¹ For a flight altitude of 300 km the light takes approximately 2 ms for its way down to the sea surface and back to the detector. During this time the platform moves ~ 15.5 m. Consequently the centres of the laser illuminated region and the detector field of view also show up a displacement of ~ 15.5 m. We assume a beam divergence of 0.3 mrad full angle. To achieve a total overlap of the laser illuminated area (90 m diameter) and the area seen by the telescope, a detector field of view of 0.4 mrad full angle is needed. Another solution would be an identical detector field of view of 0.3 mrad and an additional correction of the detector angle with respect to the lidar zenith angle of 0.05 mrad.

$$(n(z)-1) 10^6 = \left(77.46 + \frac{0.459 \mu m^2}{\lambda^2} \right) - \frac{p(z)}{T(z)} \frac{K}{hPa} - \frac{p_{H_2O}(z)}{1013 hPa} \left(43.49 - \frac{0.347 \mu m^2}{\lambda^2} \right). \quad (1)$$

For the slant path calculation we solve Fermats variation principle, stating that light always takes the shortest optical path, via the Euler-Lagrange differential equation. Implementing this solution in an integration over the altitude z the deviation x at height z_2 of a lightbeam of wavelength λ starting at z_1 at an angle $\Theta(z_1)$ can be calculated:

$$x(z_2) = x(z_1) + \int_{z_1}^{z_2} \frac{n(z_1)}{n(z)} \sin \Theta(z_1) \cdot \left(1 - \left(\frac{n(z_1)}{n(z)} \right)^2 \sin^2 \Theta(z_1) \right)^{-1/2} dz, \quad (2)$$

with $n(z) = n(T, p, p_{H_2O}, \lambda)$ being the refractive index of air following equation (1). It has been mentioned before that the movement of the platform during the time of light propagation can be compensated by a small angular correction at the detector. In the first approximation one can show that a detector at an angle of

$$\sin \Theta_{det} = \left(x_{det} - x_{probe} \right) / \int_{z_{probe}}^{z_{laser}} \frac{n(z_{probe})}{n(z)} dz, \quad (3)$$

will correct the platform movement, if x_{probe} is the centre of the laser illuminated area calculated via Eq. (2) and x_{det} is approximated by

$$x_{det} \approx 2 t v_{sat}, \quad (4)$$

with t being the elapsed time of the laser pulse from the platform to the sea surface.

Another question related to the radiative transfer in the atmosphere is the wavelength dependence of the refractive index, called dispersion. Calculating the deviation of a lightbeam, Eq. (3), for different wavelengths λ it is possible to estimate the effect of dispersion at a given nadir angle Θ_{laser} . Fig. 2 shows the difference of these deviations x_{probe} at wavelengths 685 and 308 nm. The wavelength dependence of the refractive index can be practically neglected for $\Theta_{laser} < 60^\circ$ when compared to the diameter of the illuminated area, and other disturbing effects like turbulence which has not been considered here. In another application of the simulation, it is possible to calculate complete scan patterns of a possible hydrographic lidar, using the given equations, for reasons of optimization and illustration. Fig. 3 shows such a computational scan pattern for an altitude of 300 km covering the German Bight.

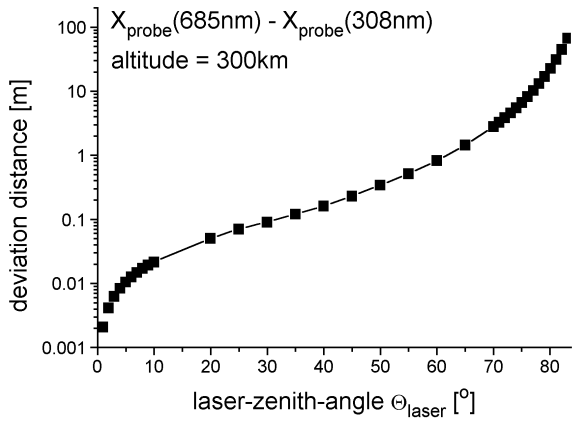


Fig. 2. Effect of dispersion for a laser beam starting at 300 km altitude at variable nadir angles Θ_{laser} measured via the deviation distance for two wavelengths.

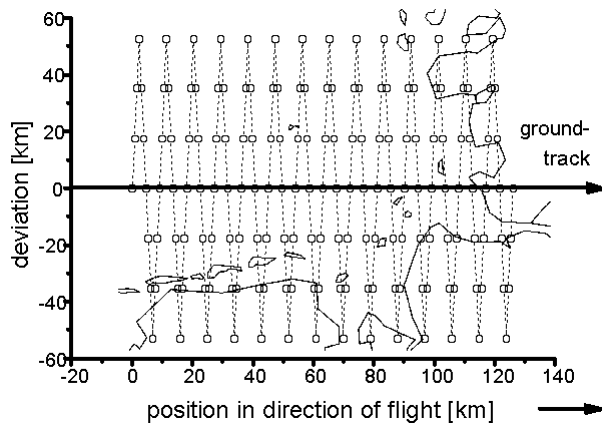


Fig. 3. Example of a scan pattern (altitude 300 km, $\lambda=355$ nm, average pulse repetition rate 10 Hz, max. scan angle 10°). A part of the German Bight was projected into the plot.

3.3 Layout of a spaceborne lidar

The model described above allows to simulate a hydrographic lidar in space under the given limitations of the approach (see Fig. 4 for illustration). That includes different scan configurations as well as footprint diameters from different beam divergencies. Flight altitudes have been chosen with respect to standard space platforms like Space Shuttle, the MIR station, or satellites on lower earth orbit. Required laser energies can be calculated by the lidar equation and have to satisfy eye safety regulations (see [2]).

An important task is the selection of the excitation wavelength for oceanic measurements. A possible laser

source is a frequency tripled Nd:YAG-laser since its 355 nm emission wavelength is in the absorption gap of ozone in the spectral region between 350 and 450 nm. Following section 2 this excitation allows for inducing gelbstoff and chlorophyll *a* fluorescence. In addition, Matvienko et al. [9] proposed to apply the 1064 nm emission for a simultaneous retrieval of atmospheric information. The Nd:YAG-laser wavelength is well known from atmospheric missions like the Lidar In-Space Technology Experiment (LITE) [13]. A combined hydrographic/atmospheric lidar would offer the possibility to combine oceanic measurements with actual atmospheric corrections, yielding quantitative results of fluorescence measurements in the surface layer of the ocean. Detection wavelengths are selected with respect to the measurable parameters and necessary baseline corrections. Table 3 summarizes some proposed features of a hydrographic lidar in space.

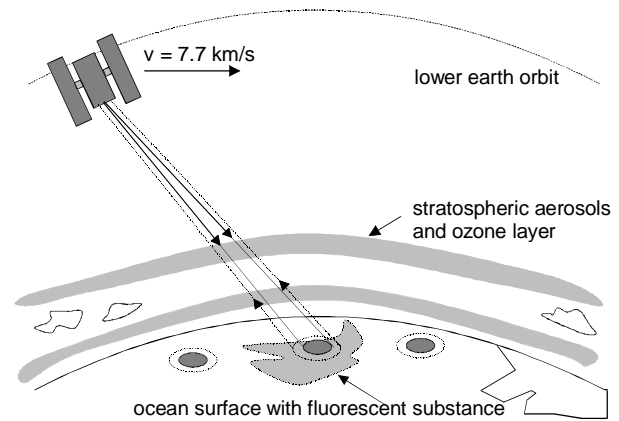


Fig. 4. Illustration of a hydrographic lidar in operation.

Table 3: Some proposed features of a hydrographic lidar in space

Operating properties			
flight altitude	100 km	or	300 km
laser beam			
divergence	0.3 mrad		
footprint diameter	30 m		90 m
pulse energy for			
s/b-ratio of 1:1	1 J		8 J
emission wavelength	355 nm (Nd:YAG-laser)		
detection channels	7 discrete: 355-380-404-430-620-685-1064 nm		
Water column parameters			
phytoplankton pigments	680 - 685 nm		
gelbstoff	max. at 420 - 450 nm		
seawater attenuation	from Raman signal		

4 DISCUSSION

We have stated that a spaceborne hydrographic lidar offers the possibility of long-term and large-scale monitoring of bio-optical components like gelbstoff and chlorophyll *a* in algae. To propose some design parameters for a possible instrument we have analysed the requirements for oceanic measurements, namely the selection of detection channels and the expected fluorescence efficiencies depending on the excitation wavelength.

The simulation of radiative transfer via a specific solution of Fermat's principle enables the optimization of lidar angle configuration. We can also show that effects caused by dispersion in the atmosphere can be neglected at small laser-zenith-angles. For an improved correction of fluorescence signals a simultaneous measurement of atmospheric parameters by a combined hydrographic/atmospheric lidar or the use of an IR-backscatter signal (e.g. 1064 nm) is proposed. It is outlined that the frequency tripled Nd:YAG-laser (355 nm) provides an effective excitation wavelength for all discussed parameters and also matches atmospheric restraints like the strong ozone-absorption below 320 nm.

Future work in this project will include evaluation of different detection wavelengths, expansion of the simulation with respect to turbulence and earth curvature, and the development of algorithms for data correction using simultaneously measured atmospheric parameters.

REFERENCES

1. Barale, V. and R. Doerffer (1993), Ocean Colour and CZCS Applications in and around Europe, in V. Barale and P.M. Schlittenhardt (Editors), Ocean Colour: Theory and Applications in a Decade of CZCS Experience, Euro courses - Rem. Sens., Vol. 3.
2. Bartsch, B., T. Braeske and R. Reuter (1993), Oceanic lidar: radiative transfer in the atmosphere at operating altitudes from 100 m to 100 km, Appl. Opt. 32, No. 33.
3. Determann, S., R. Reuter, P. Wagner and R. Willkomm (1994), Fluorescent matter in the eastern Atlantic Ocean Part 1: method of measurement and near-surface distribution, Deep-Sea Research 41, pp. 659-675.
4. Ducklow, H.W., C.A. Carlson, N.R. Bates, A.H. Knap and A.F. Michaels (1995), Dissolved organic carbon as a component of the biological pump in the North Atlantic Ocean, Phil. Trans. R. Soc. Lond. B 348, pp. 161-167.
5. Hoge, F.E., R.E. Berry and R.N. Swift (1986), Active-passive airborne ocean color measurement. 1: Instrumentation, Appl. Opt. 25, pp. 39-47.
6. Hoge, F.E., R.N. Swift and J.K. Yungel (1986), Active-passive airborne ocean color measurement. 2: Applications, Appl. Opt. 25, pp. 48-57.
7. Marra, J. (1995), Primary production in the North Atlantic: measurements, scaling, and optical determinants, Phil. Trans. R. Soc. Lond. B 348, pp. 153-160.
8. Marshall, B.R. and R.C. Smith (1990), Raman scattering and in-water ocean optical properties, Appl. Opt. 29.
9. Matvienko, G.G., G.P. Kokhanenko, M.M. Krekova, I.E. Penner and V.S. Shamanayev (1995), Representivity of the spaceborne lidar sounding of the upper sea layer, in Lidar Techniques for Remote Sensing II, SPIE Vol. 258.
10. McCartney, E.J. (1976), Optics of the Atmosphere - Scattering by Molecules and Particles, Wiley & Sons.
11. McClatchey, R.A., R.W. Fenn, J.E.A. Selby, F.E. Volz and J.S. Garing (1972), Optical Properties of the Atmosphere (Third Edition), AFCRL-72-0497, Envir. Res. Papers No. 471.
12. McClatchey, R.A. and J.E.A. Selby (1975), Atmospheric Transmittance from 0.25 to 28.5 μ m: Computer Code LOWTRAN 3, AFCRL-TR-75-0255, Envir. Res. Papers No. 513.
13. McCormick, M.P., D.M. Winkler, E.V. Browell, J.A. Coakley, C.S. Gardner, R.M. Hoff, G.S. Kent, S.H. Melfi, R.T. Menzies, C.M.R. Platt, D.A. Randall and J.A. Reagan (1993), Scientific Investigations Planned for the Lidar In-Space Technology Experiment (LITE), Bulletin of the American Meteorological Society 74, No. 2.
14. Measures, R.M. (1984), Laser Remote Sensing. Fundamentals and Applications, Wiley & Sons.
15. Reuter, R., D. Diebel and T. Hengstermann (1993), Oceanographic laser remote sensing: measurement of hydrographic parameters in the German Bight and in the Northern Adriatic Sea, International Journal of Remote Sensing 14, pp. 823-844.
16. Reuter, R., H.Wang, R. Willkomm, K. Loquay, T. Hengstermann and A. Braun (1995), A laser fluorosensor for maritime surveillance: Measurement of oil spills, EARSeL Advances in Remote Sensing 3, pp. 152-169.
17. Platt, T., S. Sathyendranath and A. Longhurst (1995), Remote sensing of primary production in the ocean: promise and fulfilment, Phil. Trans. R. Soc. Lond. B 348, pp. 191-202.